Taylor & Francis
Taylor & Francis Group

Check for updates

Characterization and quantification of railroad spiral-joint discontinuities

Ahmed A. Shabana and Hao Ling

Department of Mechanical and Industrial Engineering, University of Illinois at Chicago, Chicago, IL, USA

ABSTRACT

In this study, a new approach is proposed for the characterization and quantification of the spiral transitions in railroad vehicle system algorithms. Definitions of the super-elevation and balance speed are provided in order to have a better understanding of their variations within the space curve of the spiral segment. In order to develop this understanding, three different curves which have fundamentally different geometries are considered; a super-elevated *constant-curvature curve* with zero twist and zero vertical elevation, a vertically-elevated *helix curve* with a constant curvature and twist and zero super-elevation, and a *spiral curve* with non-zero varying-curvature, twist, super-elevation, and vertical elevation. The curve equations are developed in terms of Euler angles used by the rail industry to describe the track geometry in the computer simulations. Because the geometry of the spiral space curve can be completely defined in terms of two Euler angles only, the *horizontal-curvature* and the *vertical-development* angles; a third Euler angle referred to as the *Frenet bank angle* is written in terms of these two angles using an algebraic equation. The fact that, for given curvature and elevation angles, the Frenet bank angle cannot be treated as an independent geometric parameter is used to obtain accurate quantification of the spiral-intersection discontinuities. The severity of the twist and elevation discontinuities at the spiral intersections with the tangent and curve segments demonstrates the need for the adjustments used in practice by the rail engineers to achieve a higher degree of smoothness. In order to properly define the direction of the *centrifugal force*, a distinction is made between the super-elevation of a surface and the bank angle of a curve on the surface.

1. Introduction

A large number of investigations have been focused on many aspects of railroad vehicle mechanics and geometry, including wheel/rail contact, track geometry, suspension design, accidents and derailments, high-speed passenger and freight trains, nonlinear dynamics and stability, noise and vibration, virtual prototyping and computer simulations, field testing, etc. The track geometry, which has a significant effect on the safe operation of railroad vehicle systems, has been the subject of several investigations focused on the definition of the track layout and design (Gailienè 2012; Gilchrist 1998; Hamid et al. 1983; Kerr and El-Sibaie 1987; Klauder 2012; Klauder, Chrismer and Elkins 2002; Liu and Magel 2009). Some of these investigations are focused on the track transition discontinuity, defects, irregularities, fatigue, and geometric variations on the

railroad performance and stability (Blue and Kulakowski 1991; Magel et al. 2005; Zhang, El-Sibaie and Lee 2004; Wickens 2005). The effect of the wheel/rail interaction, suspension characteristics, braking, and critical speeds on the dynamics, stability, and derailments are other important issues that have been the subject of many studies in the railroad literature (Andersson and Abrahamsson 2002; Berghuvud 2002; De Pater 1988; Elkins and Gostling 1977; Endlicher and Lugner 1990; Grassie 1993; Handoko, Xia, and Dhanasekar 2004; Jalili et al. 2020; Kik 1992; Knothe and Grassie 1993; Knothe and Stichel 1994; Pascal and Sany 2019; True 1994). Despite the large number of investigations, railroad accidents and derailments remain common, particularly when the rail vehicle negotiates the spiral and curve sections of the track. The spiral, in particular, does not have constant geometric invariants because of the variation of the curvature, twist, and elevation. This paper builds on a previous investigation (Ling and Shabana 2020) by developing a new procedure for the characterization and quantification of the spiral-transition discontinuities. The relationship between track geometry and inertia forces that can cause derailments is also discussed in this paper.

1.1. Track geometry

For the most part, the rail track is constructed using three basic segments; *tangent*, *curve*, and *spiral*, shown in Fig. 1. The tangent segment is a straight section which has zero curvature, zero twist, and zero elevation; while the curve segment has a constant curvature and zero twist. The spiral segment, on the other hand, is designed to connect two segments which can have different curvatures and different elevations. In order to achieve a certain degree of continuity at the segment transitions, the spiral is designed to have the value of the curvature at its joints with other segments. Therefore, spirals have varying curvature, elevation, and non-zero twist. Despite the large number of derailments during curve and spiral negotiations, the spiral geometry and transition discontinuities are not well understood. Such an understanding is necessary for accurate definition of the balance speeds and wheel/rail contact forces. It is demonstrated in this paper that the direction of the centrifugal force during curve and spiral negotiations depends mainly on the direction of the vector normal to the motion-trajectory curve and not on the track super-elevation.

1.2. Numerical representation of the track geometry

In the computer simulations of railroad vehicle systems, the track geometry is numerically constructed in a track-preprocessor computer program by mesh of points along the track. At each point, the position coordinates and three Euler angles are provided. The position coordinates and Euler angles are used as field variables that depend on the distance traveled along the track.
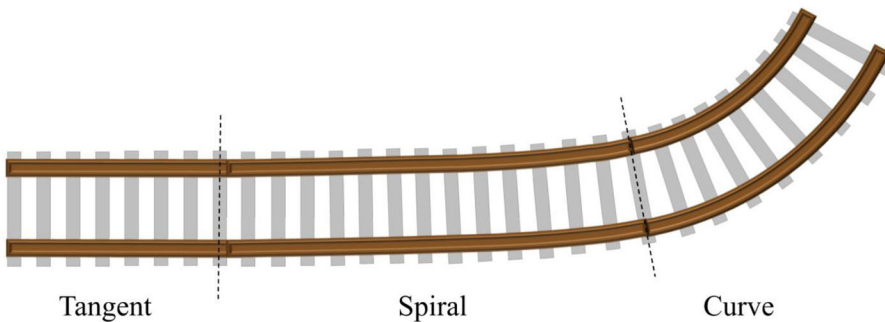

Figure 1. Track segments.

The geometry of the track is often defined using only three inputs to the track preprocessor at points of track geometry changes. These three inputs are the *horizontal curvature*, *grade*, and *super-elevation*. The grade represents a vertical elevation and its geometric interpretation is fundamentally different from the super-elevation, as will be explained in this paper. The numerical representation of the track geometry is used during the dynamic simulations for two fundamentally different purposes: (1) Definition of the track centerline geometry which is used to define the track frames used as a reference to the vehicle components; these track frames are often used in the formulation of the equations of motion and/or in the definition of the specified motion trajectories; and (2) Definition of the space curves of the rails which support the vehicle; the rail space curves are used in the formulation of the wheel/rail contact forces. It is important to point out, however, that the rail space curve geometry may significantly differ from the track centerline-curve geometry; and therefore, distinction must be made between the geometric parameters that enter into the definitions of the two sets of curves.

1.3. Track super-elevation and Frenet bank angle

In this paper distinction is made between the *track bank angle* used to define the super-elevation of the track and the approximate balance speed used in practice, and the *Frenet bank angle* used in the definition of the curve geometry and the exact balance speed. The track bank angle, referred to in this paper as ϕ_t, is a rigid-body rotation that has no effect on the geometry of the constant curve; that is, the curve geometry is invariant under the rigid-body rotation ϕ_t. This is despite the fact that this angle is used to determine the elevation of the spiral curve, and therefore, indirectly has an effect on the spiral geometry. The Frenet bank angle, on the other hand, referred to in this paper as ϕ, enters into the definition of the curve geometry and can be used to define the exact balance speed which is not a priori known, shedding light on the importance of the computer simulations for understanding the root-causes of derailments during curve negotiations. Regardless of the magnitude of the track super-elevation, a rail or motion-trajectory curve segment that lies on a plane parallel to the horizontal plane has a zero Frenet bank angle, that is, $\phi = 0$, while $\phi_t \neq 0$.

1.4. Practical considerations

As federal agencies mandate more reliance on computer simulations to develop operation and safety guidelines for transportation systems, it is necessary to develop virtual prototyping computer models that accurately describe the system physics and its complexities. Because the track geometry enters into the formulation of the wheel/rail contact forces, understanding the spiral geometry and the associated transition discontinuities is necessary to avoid curve and spiral derailments. In order to develop more realistic virtual prototyping railroad algorithms and vehicle/track models, it is important to understand the layout of the track and sources of transition discontinuities; an example of which is the discontinuity at the spiral/curve joints. The track plane must be super-elevated by the rigid-rotation angle ϕ_t in order to balance the lateral component of the centrifugal force of the vehicle during curve negotiations. On the other hand, the spiral curve is elevated and twisted in addition to having non-zero varying curvature. Unlike the curve segment, the elevation and twist of the spiral are not the result of a rigid rotation and lead to geometric changes and discontinuities at the spiral/curve junction, which produce jump discontinuities in the forces and accelerations. As previously mentioned, a curve on a track super-elevated by a non-zero rigid rotation ($\phi_t \neq 0$) can have zero Frenet bank angle ($\phi = 0$). When numerically designing the spiral geometry, both angles, ϕ and ϕ_t, must be considered, despite the fact that distinction must be made between them. The rigid-rotation angle ϕ_t can be used to define the spiral vertical elevation at the spiral/curve intersection, while the angle ϕ enters into

the definition of the curve geometry with two other angles, as discussed in this paper. The three angles cannot be treated as totally independent, and therefore, the use of a linear interpolation for the bank angle ϕ within the spiral does not have a mathematical justification. The track bank angle ϕ_t is used with a linear interpolation to define the orientation of the coordinate systems at the nodes of the track point-mesh. These coordinate systems differ from the Frenet frames of the spiral space curve by a rigid rotation about the longitudinal tangent to the spiral curve.

In railroad practice, track engineers try to smooth the discontinuity by first designing the track, which is not continuous at the spiral/curve junction, and later modify the design by using what is referred to as *doucines*; such a practice depends on the engineer skills and experience (Jean-Pierre Pascal, personal communications, 2020; Prud'home 1978). The mathematical description of such a process, however, is lacking and cannot be found in the literature. The curve discontinuity problems identified in this study explain the need for using the geometric description based on the *absolute nodal coordinate formulation* (ANCF) (Shabana 2021). A curve has only one gradient vector that cannot be used to properly account for the canting of the rail surfaces. Such a limitation can be alleviated by using the interpolations of higher order ANCF finite elements that employ more than one gradient vector. Using this approach, the discontinuities at the intersection of the surfaces of the track segments can be properly addressed, the orientation of the track frame coordinates can be consistently evaluated, and the limitations of the one-dimensional curve theory in the numerical description of the track geometry can be avoided (Shabana 2021).

1.5. Track geometry and motion trajectories

The actual magnitude and direction of the centrifugal inertia forces depend on the loads and operating conditions of the rail vehicles. Nonetheless, because such conditions vary for different trains that negotiate the same fixed track; operation guidelines, such as balance speeds, are developed based on the predefined track geometry. In developing some of these operation guidelines, the vehicle is assumed to trace a horizontal circle when negotiating a constant curve. Such an assumption leads to a centrifugal inertia force that lies in a horizontal plane. Because the actual motion-trajectory curves and directions of the centrifugal forces are not a priori known, this assumption has been considered a good approximation in the design of the track layout.

Because the track super-elevation is designed to create a gravity force component that balances the lateral component of the centrifugal force resulting from curve negotiations; quantifying the bank-angle discontinuities at the track transitions is necessary for understanding the discontinuities in the direction of the centrifugal force. Nonetheless, the direction of the centrifugal force is independent of the track super-elevation angle ϕ_t and depends on the Frenet bank angle ϕ as discussed in this paper. Therefore, in this study, particular attention is given to the general definition of the centrifugal force in order to understand the effect of the discontinuity in the bank angle ϕ on the railroad-vehicle dynamics. To this end, a distinction is made between the super-elevation of a surface and the super-elevation of the osculating plane which defines the direction of the tangent and normal to the motion-trajectory curve. The vector normal to the actual motion-trajectory curve defines the direction of the *centrifugal inertia force*.

2. Scope and contributions of this investigation

This paper introduces a new procedure for the characterization and quantification of the spiral/tangent and spiral/curve intersection discontinuities. The paper is focused on the numerical description of the track geometry used in railroad vehicle system algorithms. The severity of the intersection discontinuities of the spiral space curve, quantified analytically in this study, sheds
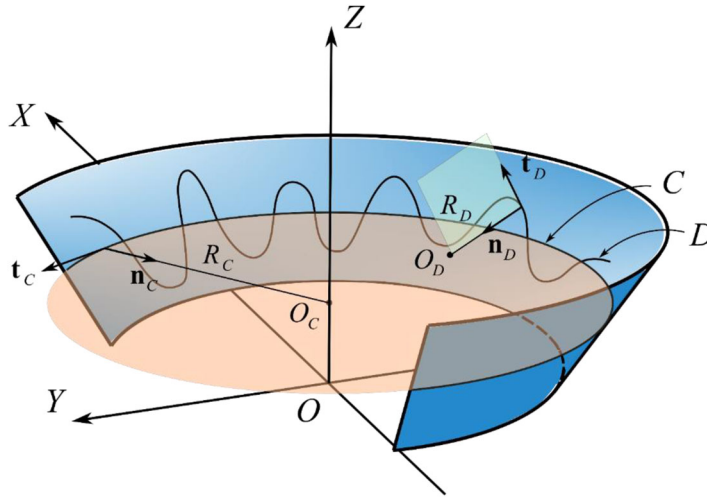
Figure 2. Track and motion-trajectory planes.

light on the significance of the smoothing process used in practice (Jean-Pierre Pascal, personal communications, 2020; Prud'home 1978).

2.1. Geometry concepts and definition of the centrifugal force

In order to explain the importance of accurate definition of the track super-elevation and Frenet bank angle, the simple example of the super-elevated conic surface shown in Fig. 2 is considered. The figure shows a circular curve C that lies on the horizontal plane; that is, this circular curve is the intersection of the conic surface and a horizontal planar surface. If a mass strictly follows this horizontal circular curve, the centrifugal force remains in the horizontal plane along the vector $\mathbf{n}_C$ normal to curve. If the mass, on the other hand, moves laterally in addition to the forward motion on the conic surface, the mass traces another curve D, shown in the figure. This lateral displacement in railroad systems can represent hunting oscillations, sliding toward the low rail, and/or lateral wheel climb displacements. The figure shows the actual *motion plane* at an arbitrary point on curve D; this is the *osculating plane* formed by the tangent vector $\mathbf{t}_D$ and the normal vector $\mathbf{n}_D$. This motion plane is, in general, different from the plane tangent to the surface, that is, the normal vector $\mathbf{n}_D$ does not in general lie on the tangent plane of the surface which has the curve D. As explained in this paper, the direction of the centrifugal force is always along the normal vector $\mathbf{n}_D$, which does not always lie in the horizontal plane. The curvature of the curve D resulting from the lateral motion cannot always be assumed small, particularly at higher speeds.

Because of the difference in the elevations of the conic surface and the osculating plane, which represents the actual motion plane that contains the velocity and acceleration vectors; distinction must be made between the *track super-elevation* and the super-elevation of the motion (osculating) plane which defines correctly the direction of the centrifugal force. The track (displacement-velocity) plane and the osculating (velocity-acceleration) plane share the vector tangent to the motion-trajectory curve, and therefore, they differ by a single rotation about the tangent vector $\mathbf{t}_D$. The geometry of the actual motion-trajectory curve can be significantly different from the geometry of the desired-motion circular curve. In this study, whenever referring to the motion-trajectory curve, the bank angle used, ϕ, refers to the super-elevation of the motion osculating plane and not the track super-elevation angle ϕ_t. These two planes may temporarily coincide, and in this special case, the centrifugal force is in the plane of the super-elevated track; unless the

motion is constrained to strictly follow a horizontal circle. The analysis presented in this paper demonstrates that the expression of the balance speed using the track super-elevation is an approximation based on the assumption that the centrifugal force remains in the horizontal plane. Nonetheless, by maintaining the track super-elevation below 6 or 7 inches, this approximation is considered a good approximation. One important observation from Fig. 2, discussed further in the appendix, is that the variation of the Curve-C curvature angle with respect to the arc length of curve D is always smaller than the variation of the same angle with respect to the arc length of the circle C.

2.2. Contributions of this study

The specific contributions of this paper can be summarized as follows:

1. A new approach for the characterization and quantification of the transition discontinuities of the spiral space curve is developed. This approach is based on analytical description of the track based on the differential-geometry theory of curves. In developing this approach distinction is made between the geometry of the spiral space curve, and the geometry of the track centerline that defines the orientations of the coordinate systems used to define the track frames.
2. Definitions and interpretation of the spiral super-elevation and balance speed are provided to better understand their variation within the spiral. To this end, three different curves which have fundamentally different geometries are considered. The first is a super-elevated *constant-curvature curve* with zero twist and zero vertical-elevation. The second is a vertically-elevated *helix curve* with constant curvature and twist, and zero bank angle. The third is a *spiral curve* with non-constant curvature, twist, super-elevation, and vertical-elevation.
3. The curve equations are developed using the Euler-angle sequence used by the industry to describe the track geometry. Because the three Euler angles used to describe the space curve geometry are not independent, the spiral geometry can be completely defined in terms of two track angles only, the *horizontal-curvature* and the *vertical-development* angles; and consequently, the Frenet bank angle ϕ can be written in terms of these two angles using an algebraic equation.
4. The significance of the bank-angle variation within the spiral is further explained by outlining a procedure for evaluating the direction of the *centrifugal force*. The direction of the centrifugal force is defined by the direction of the unit normal to the motion-trajectory curve.
5. In view of the closed-form equations presented in this paper, the numerical results obtained explain the problems associated with using independent linear interpolation of the bank angle if such an angle is interpreted as the bank angle ϕ that enters into the definition of the curve geometry used to determine the direction of the centrifugal force.

3. Inertia force and curve geometry

When a surface is super-elevated, the direction of the centrifugal force of a mass on the surface remains in the horizontal plane if the mass is constrained to strictly trace a circular curve that lies in a plane parallel to the horizontal plane. Nonetheless, such a scenario of constrained motion is difficult to achieve in practice, particularly when a vehicle negotiates a spiral segment of the track. In order to develop an accurate definition of the balance speed, it is necessary to properly define the direction of the centrifugal force. To this end, one needs to distinguish between the surface and motion-trajectory curve super-elevations, and their bank angles. A space curve is defined using one parameter, which can be selected to be the arc length parameter s. The position of an arbitrary point on the curve in a global fixed coordinate system XYZ can be written in

terms of the curve parameter as $\mathbf{r} = \mathbf{r}(s)$. A mass that traces this curve has the absolute velocity $\dot{\mathbf{r}} = \dot{\mathbf{r}}(s) = \mathbf{r}_s \dot{s}$, where $\dot{a}$ denotes the time derivative of a with respect to time t, and $\mathbf{r}_s = \partial \mathbf{r}/\partial s$ is the unit vector tangent to the curve.

3.1. Normal vector and inertia force

The track super-elevation is designed to create a gravity force component that balances the lateral component of the centrifugal force resulting from curve negotiations. Discontinuities of the bank angle at the spiral transitions lead to discontinuities in the direction of the centrifugal force. When a mass negotiates a curve, the absolute acceleration vector is written as $\ddot{\mathbf{r}} = \ddot{\mathbf{r}}(s) = \mathbf{r}_{ss}(\dot{s})^2 + \mathbf{r}_s \ddot{s}$, where $\mathbf{r}_{ss}$ is the curvature vector. This equation can be written as $\ddot{\mathbf{r}}(s) = \kappa \mathbf{n}(\dot{s})^2 + \mathbf{r}_s \ddot{s}$; where $\kappa(s) = |\mathbf{r}_{ss}| = 1/R(s)$ is the curve curvature defined as the norm of the curvature vector $\mathbf{r}_{ss}$, R is the radius of curvature, and $\mathbf{n}$ is the unit vector normal to the curve. The vector $\ddot{\mathbf{r}}(s) = \kappa \mathbf{n}(\dot{s})^2 + \mathbf{r}_s \ddot{s}$ has two components along two orthogonal vectors; the unit tangent vector $\mathbf{r}_s$ and the unit normal vector $\mathbf{n}$. The inertia force of the mass m can then be written as

$$\mathbf{F}_i = m\ddot{\mathbf{r}} = -\mathbf{F}_{ic} + \mathbf{F}_{it} = m\left(\kappa \mathbf{n}(\dot{s})^2 + \mathbf{r}_s \ddot{s}\right) \tag{1}$$

where $\mathbf{F}_{ic} = -\kappa m \mathbf{n}(\dot{s})^2 = -(m(\dot{s})^2/R)\mathbf{n}$ is the centrifugal inertia force vector, and $\mathbf{F}_{it} = m\mathbf{r}_s \ddot{s}$ is the inertia force vector in the tangential direction. If the vehicle is negotiating the curve with a constant forward velocity $\dot{s} = V$, $\ddot{s} = 0$, and consequently, the tangential component of the inertia force is identically equal to zero. That is, $\mathbf{F}_{it} = 0$.

The simple analysis presented in this section demonstrates that the centrifugal force is along the direction of the normal to the motion-trajectory curve. A motion-trajectory curve defined on a super-elevated surface can have a normal vector with direction that is independent of the surface inclination. For example, the motion of a mass can be constrained to trace a horizontal circular path on a curved and super-elevated surface, and in this case, the centrifugal force remains in the horizontal plane regardless of the curvature and the super-elevation of the surface. For this reason, distinction is made in this paper between the super-elevation of a surface and the super-elevation or bank angle of a curve on the surface. The super-elevation of the curve is measured by the direction of the unit vector normal to the curve, which defines the direction of the centrifugal force.

3.2. Euler-angle representation

Unit vectors tangent and normal to the curve can be expressed in terms of Euler angles. The sequence of Euler angles used in the railroad literature to describe the track geometry is $Z, -Y, -X$. The three Euler angles used in this sequence are, respectively, the *horizontal-curvature angle* ψ, the *vertical-development angle* θ, and the *bank angle* ϕ (Klauder 2012; Klauder, Chrismer and Elkins 2002; Shabana, Zaazaa and Sugiyama 2008; Shabana 2021). Because of using this sequence in which the bank angle represents the last rotation, addition and interpolation of the bank angle is allowed. The unit tangent and unit normal vectors can be written, respectively, in terms of the three Euler angles as (Ling and Shabana 2020; Shabana and Ling 2019)

$$\mathbf{r}_s = \begin{bmatrix} \cos\psi\cos\theta \\ \sin\psi\cos\theta \\ \sin\theta \end{bmatrix}, \quad \mathbf{n} = \begin{bmatrix} -\sin\psi\cos\phi + \cos\psi\sin\theta\sin\phi \\ \cos\psi\cos\phi + \sin\psi\sin\theta\sin\phi \\ -\cos\theta\sin\phi \end{bmatrix} \tag{2}$$

The three Euler angles can be written in terms of the curvature κ and torsion τ of the curve using the differential relationships (Ling and Shabana 2020)

$$\psi' = \kappa \cos \phi / \cos \theta, \quad \theta' = -\kappa \sin \phi, \quad \phi' = \kappa \tan \theta \cos \phi - \tau \qquad (3)$$

In this equation, $a' = \partial a / \partial s$. The above differential equations can be obtained by differentiating the unit tangent with respect to the arc length and equating the results to the columns of the Euler-angle transformation matrix (Shabana, Zaazaa and Sugiyama 2008; Shabana 2021). It is important to point out that rigid rotations are not governed by these differential equations. The inverse relationships are

$$\kappa = \psi' \cos \phi \cos \theta - \theta' \sin \phi, \quad \tau = \psi' \sin \theta - \phi' \qquad (4)$$

Using these differential relationships, one can show that the curvature vector can be written as

$$\mathbf{r}_{ss} = \begin{bmatrix} -\psi' \sin \psi \cos \theta - \theta' \cos \psi \sin \theta \\ \psi' \cos \psi \cos \theta - \theta' \sin \psi \sin \theta \\ \theta' \cos \theta \end{bmatrix} = \psi' \cos \theta \begin{bmatrix} -\sin \psi \\ \cos \psi \\ 0 \end{bmatrix} + \theta' \begin{bmatrix} -\cos \psi \sin \theta \\ -\sin \psi \sin \theta \\ \cos \theta \end{bmatrix} \qquad (5)$$

That is, the curvature vector has a component $\psi' \cos \theta$ along the unit vector $\mathbf{v}_h = \begin{bmatrix} -\sin \psi & \cos \psi & 0 \end{bmatrix}^T$ defined on the horizontal plane, and a component θ' along the unit vector $\mathbf{v}_n = \begin{bmatrix} -\cos \psi \sin \theta & -\sin \psi \sin \theta & \cos \theta \end{bmatrix}^T$ which is normal to $\mathbf{v}_h$. For this reason, ψ is called the horizontal-curvature angle and θ the vertical-development angle. In railroad vehicle systems, the horizontal curvature is defined as $C_H = \psi' / \cos \theta$, and the vertical curvature is defined as $C_V = \theta'$ (Shabana, Zaazaa and Sugiyama 2008; Shabana 2021). The curve curvature can be written in terms of the curvature components as

$$\kappa = \sqrt{(C_H \cos^2 \theta)^2 + (\theta')^2} = \sqrt{(\psi' \cos \theta)^2 + (C_V)^2} \qquad (6)$$

The curvature of the curve enters into the definition of the centrifugal inertia forces and the balance speed. Because a curve can be twisted while the angle ϕ is zero, ϕ is not called in this paper the twist angle despite the fact that it enters into the definition of the curve torsion (twist). It is also important to note that the normal vector $\mathbf{n}$ and the centrifugal force $\mathbf{F}_{ic}$ remain in the horizontal plane if the bank angle ϕ is zero.

4. Balance speed and implementation issues

In this section, a general expression for the balance speed applicable to the spiral geometry is presented. It is important to note that in practice the balance speed is defined based on the assumption that the vehicle negotiates a constant curve that lies in a plane parallel to the horizontal plane. The track super-elevation is designed in order to balance the lateral component of the centrifugal force using the lateral component of the gravity force. In a realistic motion scenario, however, the vehicle motion trajectory deviates from the horizontal curve, and consequently, the actual direction and magnitude of the centrifugal forces differ from those used in the definition of the balance speed. Therefore, the balance speed used in practice can be viewed as an approximation that can be justified since the actual motion trajectories are not a priori known. This fact explains the need for the computer simulations that can be used to provide explanation of the root causes of derailments.

4.1. Balance speed

The super-elevation is used to create a component of the gravity force $\mathbf{F}_g = \begin{bmatrix} 0 & 0 & -mg \end{bmatrix}^T$ that balances the lateral component of the centrifugal force vector $\mathbf{F}_{ic}$ which acts in a direction along the normal to the motion-trajectory curve, where g is the gravity constant. Equation 2, however,

shows that if the bank angle ϕ is zero, the curve normal remains in the horizontal plane regardless of the value of the vertical-development angle θ. That is, a curve, such as the helix, can be vertically elevated and twisted, but not super-elevated. Twisting a curve can lead to vertical curvature C_V and vertical-development angle θ, but not necessarily to a bank angle. Equation 4 shows that non-zero torsion does not imply non-zero bank angle.

In general, the super-elevation and force equilibrium along the normal to the curve are used to define the balance speed that ensures a safe operation of the vehicle. Therefore, the balance speed, in its most general form, can be determined from the equilibrium relationship $(\mathbf{F}_g^T \mathbf{n})\mathbf{n} + \mathbf{F}_{ic} = 0$; which leads to $m(\dot{s}_b)^2/R = mg \cos \theta \sin \phi$, where $\dot{s}_b$ is the *balance speed*. This equation leads to

$$\dot{s}_b = \sqrt{gR \cos \theta \sin \phi} \qquad (7)$$

In this definition of the balance speed, the motion-trajectory curve Frenet bank angle ϕ is used and not the track super-elevation angle ϕ_t. It is clear that if $\phi = 0$, the balance speed is zero, regardless of the value of the vertical-development angle θ. In the case of the spiral, the vertical-development angle θ is not zero in general. The preceding equation also demonstrates the fundamental difference between the general concept underlying the development of this equation and the concept used in practice to define the balance speed, as will be further discussed in this paper. Using the preceding equation, the centrifugal force, and not only its lateral component, can be entirely balanced by the component of the gravity force along the normal to curve.

4.2. Important implementation issue

The parametric-form equation of the spiral $\mathbf{r} = \mathbf{r}(s)$ leads to $d\mathbf{r} = \mathbf{r}_s(s)ds$. That is, given the tangent vector $\mathbf{r}_s$ in terms of Euler angles, the differential equation $d\mathbf{r} = \mathbf{r}_s(s)ds$ can be integrated to determine the position coordinates of an arbitrary point on the spiral curve. It is important to note that the unit tangent vector $\mathbf{r}_s = \begin{bmatrix} \cos \psi \cos \theta & \sin \psi \cos \theta & \sin \theta \end{bmatrix}^T$ in Eq. 2 does not depend on the bank angle. That is, the position coordinates of an arbitrary point on the spiral and its geometry are completely defined in terms of the angles ψ and θ only using the equation

$$\mathbf{r}(s) = \mathbf{r}_o + \int_s \mathbf{r}_s ds = \mathbf{r}_o + \int_s \begin{bmatrix} \cos \psi \cos \theta & \sin \psi \cos \theta & \sin \theta \end{bmatrix}^T ds \qquad (8)$$

where $\mathbf{r}_o$ is the position of the origin of the curve coordinates system. This definition of the position coordinates is consistent with the fact that the curve geometry can be described in terms of two independent Euler angles only (Ling and Shabana 2020; Shabana and Ling 2019); and is consistent with the differential-geometry theory of curves that a curve is completely defined by its curvature and torsion (Do Carmo 1976; Goetz 1970; Kreyszig 1991). This important observation implies that the Frenet bank angle cannot be considered as an independent geometric variable.

4.3. Track super-elevation

In order to understand the significance of the observation made in this section, we consider a tangent and curve segments connected by a spiral segment. The flanges of the wheels ensure that the motion trajectories of the wheelsets remain within a limit. The definition of the balance speed used in practice is based on the assumption that the vehicle negotiates curves that lie in planes parallel to the horizontal plane, and consequently, the lateral displacement and its effect on the actual motion trajectories are not considered. This is equivalent to using the assumption $\phi = 0$.

In order to super-elevate the track with the rigid rotation ϕ_t required to define the balance speed in practice, the end of the spiral at its connection with the curve is elevated as well.

Because the spiral can be twisted, the amount of vertical-elevation and super-elevation at the spiral ends need to be quantified in order to understand the discontinuities at the spiral joints. Due to the fact that the tangent vector is not function of ϕ, the track bank angle ϕ_t can be used to define the coordinates of the spiral endpoint (Ling and Shabana 2020). The vertical coordinate of the spiral at its two ends with the tangent and curve segments can be used to define the vertical-elevation (grade). Using this vertical-elevation and the assumption of constant vertical curvature C_V, the vertical-development angle θ can be determined from the integration of the third component of Eq. 8 (Ling and Shabana 2020). Knowing $\theta = \theta(s)$ and the curvature angle $\psi = \psi(s)$, the spiral geometry can be completely defined. Furthermore, knowing the angles θ and ψ, the Frenet bank angle ϕ can be determined using the first two equations of Eq. 3 as (Ling and Shabana 2020)

$$\phi = \tan^{-1}\left(-C_V/C_H \cos^2\theta\right) \qquad (9)$$

This algebraic equation will allow quantifying the discontinuities and will explain the abrupt change in the direction of the normal at the spiral intersections. This abrupt change can lead to significant increase in the lateral forces when a vehicle enters, negotiates, and leaves the spiral.

In the following three sections, three different curves with three different geometries are considered in order to shed light on the effect of the geometry on the balance speed. The first is a circular curve with zero vertical elevation and twist. The second is a vertically-elevated helix curve with constant curvature and twist, and zero Frenet bank angle. The third is a curved, twisted, super-elevated, and vertically-elevated spiral.

5. Circular curve

Regardless of the amount of the track super-elevation defined by a bank angle ϕ_t, the motion-trajectory curve traced by a vehicle can have a geometry that does not depend on the track super-elevation. For example, as shown in Fig. 3a, a track can be super-elevated by the bank angle ϕ_t while a vehicle traces a circular curve that lies in a plane parallel to the horizontal plane. The horizontal circular curve has a Frenet bank angle ϕ that is identically zero. Therefore, distinction must be made between the track super-elevation and the Frenet bank angle of the motion-trajectory curves. This distinction is of fundamental importance in understanding the discontinuities at the track transitions and also in understanding the problems associated with interpreting the Frenet bank angle ϕ as an independent angle that enters into the definition of the spiral space-curve geometry. The bank angle ϕ_t of the track can be used to only define the vertical elevation
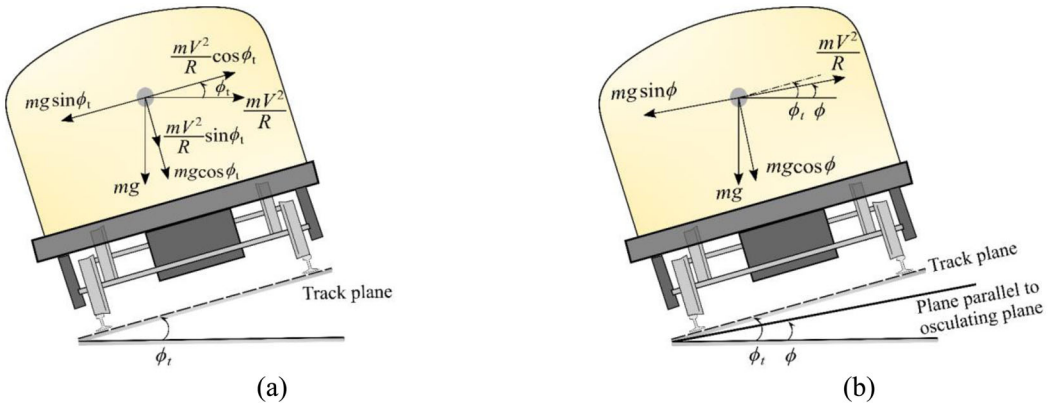
Figure 3. Super-elevation and centrifugal forces ($V = \dot{s}$); (a) Horizontal-curve negotiation with zero Frenet bank angle, $\phi = 0$; (b) Motion-trajectory-curve with nonzero Frenet bank angle, $\phi \neq 0$. (Vectors in this figure are not drawn to scale.)

of the spiral at the spiral/curve transition, as described in this paper; and it is also used with a linear interpolation to define the track frames at the nodes to properly account for the track super-elevation in the spiral section. The spiral vertical elevation at the intersection can be used to define the vertical-development angle θ. Knowing the horizontal curvature C_H, which is assumed to vary linearly within the spiral, the horizontal-curvature angle ψ can be determined. The two angles ψ and θ can be used to define the spiral Frenet bank angle ϕ.

Furthermore, in defining the direction of the centrifugal force, distinction is made between the super-elevation of a surface and the Frenet bank angles of and direction of the normal to the curves on the surface. On a super-elevated track, the motion of the vehicle can be constrained to trace a circular curve that lies in a *horizontal-plane*, regardless of the amount of curvature and super-elevation of the surface. This strict condition of negotiating a horizontal curve cannot always be met in practice because of the lateral oscillations. Because the direction of the centrifugal force is always along the unit vector normal to the motion-trajectory curve, one needs to distinguish between the super-elevations of the surface and the *motion plane* formed by the tangent and normal vectors of the motion-trajectory curve in order to be able to accurately define the balance speed.

5.1. Horizontal-plane curve

The equation of a planar circular curve can be written as $\mathbf{r}(s) = \begin{bmatrix} R\sin\psi & -R\cos\psi & z_c \end{bmatrix}^T$, where R is the radius of curvature of the curve, ψ is the horizontal curvature angle, and z_c is a constant that defines the curve vertical translation. The unit tangent to the curve is defined as $\mathbf{r}_s(s) = \psi' R \begin{bmatrix} \cos\psi & \sin\psi & 0 \end{bmatrix}^T$. Because $\psi = s/R$, $\psi' R = 1$, and one can show that $\mathbf{r}_s(s) = \begin{bmatrix} \cos\psi & \sin\psi & 0 \end{bmatrix}^T$ is indeed a unit vector. The curvature vector of the circular curve is $\mathbf{r}_{ss}(s) = \psi' \begin{bmatrix} -\sin\psi & \cos\psi & 0 \end{bmatrix}^T$. In this case, the curvature of the curve is defined as $\kappa = \psi' = 1/R$, and the unit normal vector is $\mathbf{n} = \begin{bmatrix} -\sin\psi & \cos\psi & 0 \end{bmatrix}^T$. It is clear in this special case of a horizontal-plane circular curve that the centrifugal force is in the horizontal plane and in the case of zero Frenet bank angle ϕ such a centrifugal force cannot be entirely balanced by the gravity force since $\mathbf{F}_g^T \mathbf{n} = 0$. That is, the gravity force has no component along the curve normal that defines the direction of the centrifugal force. For this reason, the track super-elevation by an angle ϕ_t creates a gravity force component that balances the lateral component of the centrifugal force.

5.2. Super-elevated track

As previously mentioned, a vehicle can negotiate a horizontal curve on a super-elevated track. In this case, the axis of rotation remains vertical and the normal to the motion-trajectory curve and the centrifugal force remain in the horizontal plane. That is, the super-elevation does not lead to a change in the Frenet bank angle of the curve. However, in the case of the spiral curve, ϕ varies with the arc length and cannot be assumed zero, and therefore, the direction of the normal to the curve varies along the curve and the curve normal and centrifugal force do not remain in the horizontal plane. Therefore, in the case of a track super-elevated by a constant angle ϕ_t, there are two motion scenarios that can be considered; in the first scenario discussed in this subsection, the vehicle mass center negotiates a horizontal-plane curve; while in the second scenario, discussed in the following subsection, the vehicle negotiates a curve on the super-elevated surface, which has a Frenet bank angle $\phi = \phi(s)$ that defines the direction of the normal to the curve; this second scenario cannot be ignored because it represents the spiral geometry and also represents the actual motion-trajectory curve if motion in the horizontal plane cannot be ensured.

In the first scenario of a *horizontal-plane curve* defined on a super-elevated track, shown in Fig. 3a, the normal to the curve remains in the horizontal plane and takes the form $\mathbf{n} = \begin{bmatrix} -\sin\psi & \cos\psi & 0 \end{bmatrix}^T$ as previously discussed in this section. In this case, $\phi = 0$ and $\phi_t \neq 0$. The centrifugal force in this case is along the normal to the curve. If the vehicle strictly traces this horizontal curve and the lateral constraint force is assumed to be zero, one has the lateral force equilibrium condition $mg\sin\phi_t = (m(\dot{s}_b)^2/R)\cos\phi_t$, which defines the balance speed as $\dot{s}_b = \sqrt{Rg\tan\phi_t}$. In this case, the balance speed is defined in terms of ϕ_t and not in terms of ϕ. Furthermore, the equilibrium condition used to obtain this balance speed, which is based on the predefined track geometry and not on the actual-motion trajectory curve, does not entirely balance the centrifugal force. To mathematically ensure that the vertical and lateral displacements are always zero such that the lateral force equilibrium is strictly satisfied, Lagrange-D'Alembert's principle and the embedding technique must be used to systematically reduce the number of coordinates to one coordinate that describes the forward motion of the vehicle. In this case of one-degree-of-freedom system, the normal reaction force acting on the super-elevated track plane is equal to $N_n = mg\cos\phi_t + (m(\dot{s}_b)^2/R)\sin\phi_t$, where N_n is the constraint force normal to the super-elevated plane; that is the centrifugal force contributes to the axle load on the super-elevated track. Using the lateral force equilibrium, the reaction force on the super-elevated plane can be written as $N_l = mg\sin\phi_t - (m(\dot{s}_b)^2/R)\cos\phi_t$, where N_l is the constraint force in the lateral direction.

5.3. Super-elevated motion plane

The horizontal-plane circular curve can be defined as the curve resulting from the intersection of a horizontal plane and the super-elevated track plane. This condition is not met in the case of the spiral geometry in which $\phi = \phi(s)$ varies along the twisted curve; nor in the case of more general motion-trajectory curve entirely defined in the track plane and not in the horizontal plane. In this case, the direction of the centrifugal force, shown in Fig. 3b, is different from the case of the horizontal-plane curve. It is important to reiterate that in Fig. 3b, the angle $\phi = \phi(s)$ defines the direction of the normal to the motion-trajectory curve and not the track super-elevation defined by the rigid-rotation angle ϕ_t. That is, the osculating plane is super-elevated by the angle $\phi = \phi(s)$, and as previously mentioned, while the motion-trajectory curve lies in the track plane, the osculating-plane and the track-plane bank angles differ by $\phi_t - \phi$, as discussed further in the appendix.

5.4. More general displacement

Figure 3 explains the use of the super-elevation to balance the centrifugal force by the gravity force component along the normal to the circular curve in the two different cases discussed above. The figure depicts two different scenarios that depend on the trajectory of the center of mass of the vehicle when negotiating a super-elevated track. In Fig. 3b, the vehicle center of mass is assumed to follow a curve which has a normal that does not lie in the horizontal plane and the balance speed in the case of zero vertical-development angle is defined by the equation $\dot{s}_b = \sqrt{gR\sin\phi}$, as previously discussed, where $\phi = \phi(s)$ defines the direction of the normal to the motion-trajectory curve. In case of negotiating a horizontal circle, the unit normal to the curve lies in the horizontal plane and the direction of the centrifugal force is as shown in Fig. 3a. Using a force balance in the lateral direction as previously discussed, one has $(mV^2/R)\cos\phi_t = mg\sin\phi_t$, which defines the balance speed as $\dot{s}_b = \sqrt{Rg\tan\phi_t}$. In most practical railroad applications, the definitions of the balance speeds in the two different scenarios shown in Fig. 3 should

not deviate significantly. Furthermore, as previously mentioned, the track (displacement-velocity) plane and the osculating (velocity-acceleration) plane share the vector tangent to the motion-trajectory curve, and therefore, the instantaneous difference between them is the difference between their bank angles.

6. Centrifugal force of helix curves

In order to better understand the spiral geometry, its geometric discontinuities, the role of the Frenet bank angle, and the effect of the orientation of the curve normal vector; another simple, yet extreme, example, a *helix curve*, is considered in this section. The helix curve has a constant curvature and constant twist, it is vertically-elevated, but not super-elevated and has zero Frenet bank angle, that is, $\phi = \phi_t = 0$. The parametric equation of a circular helix curve, as the one shown in Fig. 4, is defined as

$$\mathbf{r}(s) = \begin{bmatrix} a\cos\alpha & a\sin\alpha & b\alpha \end{bmatrix}^T \tag{10}$$

where $\alpha = s/\sqrt{a^2 + b^2}$, s is the arc length parameter, a is the helix radius, and b/a is the slope of the helix. Using the preceding equation, it can be shown that the curvature κ and torsion τ are constant and defined, respectively, as $\kappa = |a|/(a^2 + b^2)$ and $\tau = b/(a^2 + b^2)$. Using these equations, C_H and θ can be written in terms of a and b, respectively, as $C_H = \pm 1/a$ and $\tan\theta = \pm b/a$. While this helix curve is not a planar curve, the vertical curvature $C_V = 0$, the Frenet bank angle $\phi = 0$, and the vertical-development angle θ is constant. It is important to note that the Frenet bank angle ϕ is zero despite the fact that the curve is twisted.

The unit tangent vector of the helix curve is $\partial\mathbf{r}/\partial s = (1/r)\begin{bmatrix} -a\sin(s/r) & a\cos(s/r) & b \end{bmatrix}^T$, where $r = \sqrt{a^2 + b^2}$. Using this tangent vector, the curvature vector can be evaluated as $\mathbf{r}_{ss} = \partial^2\mathbf{r}/\partial s^2 = -(a/r^2)\begin{bmatrix} \cos(s/r) & \sin(s/r) & 0 \end{bmatrix}^T$, which defines the unit normal to the curve as $\mathbf{n} = -\begin{bmatrix} \cos(s/r) & \sin(s/r) & 0 \end{bmatrix}^T$. If a mass traces the helix curve with a constant forward velocity $\dot{s}$, the vehicle absolute acceleration is $\mathbf{a} = \mathbf{r}_{ss}\dot{s}^2 = \kappa\mathbf{n}\dot{s}^2 = -(a/r^2)\dot{s}^2\begin{bmatrix} \cos(s/r) & \sin(s/r) & 0 \end{bmatrix}^T$.
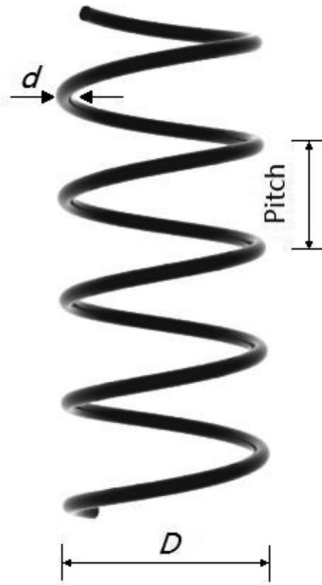

Figure 4. Helix curve. $a = (D - d)/2$, $b = \text{pitch}/2\pi$, D is the outer diameter, d is wire diameter.

Clearly, for the vertically-elevated, curved, and twisted helix the normal and acceleration vectors lie in the horizontal plane and the centrifugal force has no component along the vertical axis.

7. Spiral geometry and discontinuities

The spiral segment has a geometry that is fundamentally different from the geometry of the curve and helix examples discussed in the preceding two sections. The spiral segment is curved, twisted, vertically-elevated, and super-elevated. For a spiral segment that connects a tangent segment, which is not vertically elevated, to a curve segment; the Frenet bank angle ϕ that enters into the definition of the spiral space curve is a field variable, that is, $\phi = \phi(s)$. If the curve segment is a horizontal curve on a super-elevated track, $\phi_t \neq 0$ for this section of the track, while $\phi = 0$ for the circular horizontal curve if the effect of the cant is not taken into consideration. Because ϕ_t defines the vertical elevation of the spiral at the transition point, the vertical-development angle θ can be determined and used with the horizontal-curvature angle ψ to define the spiral bank angle $\phi = \phi(s)$.

The super-elevation and curvature within the spiral are not constant, and therefore, a constant balance speed cannot, in general, be defined when the vehicle negotiates the spiral sections of the track. Furthermore, the assumption made in the literature of linearly-varying bank angle cannot, in general, be applied to the Frenet bank angle because the use of such an assumption is not consistent with the theory of curves (Klauder, Chrismer and Elkins 2002; Shabana, Zaazaa and Sugiyama 2008; Shabana 2021). That is a curve cannot be defined using three independent geometric parameters. The spiral geometry is governed by the general equations presented in Section 3. These equations can be used to shed light on the degree of discontinuities at the spiral/tangent and spiral/curve intersections. Because of the lack of approaches for characterizing and quantifying these discontinuities and lack of understanding the variation of the super-elevation and vertical-elevation within the spiral segments, developing credible operation and safety guidelines to avoid serious accidents and derailments is not possible.

The numerical results presented in this section are obtained using the tangent-spiral-curve-assembly track data presented in Table 1 (Ling and Shabana 2020). These results show high degree of discontinuities and should be interpreted qualitatively because the geometric analysis developed in this paper does not account for some practical considerations used in the actual lay-out of the track.

7.1. Spiral vertical- and super-elevations

When a spiral is used to connect tangent and curve segments, for example; the curvature, twist, super-elevation, and vertical-elevation at the tangent/spiral intersection are assumed zeros. On the other hand, the track at the spiral/curve intersection has non-zero curvature, zero twist, zero vertical-elevation, and nonzero super-elevation as defined by the angle ϕ_t. Because of the super-elevation of the track by a rigid rotation ϕ_t which does not affect the curve geometry, the position coordinates of the spiral/curve intersection point can be determined using simple kinematics. The position coordinates of the point of the spiral/tangent intersection are also assumed to be known. Knowing these position coordinates at the two intersection points and using the assumption of constant vertical curvature C_V within the spiral, the vertical-elevation angle θ can be determined

Table 1. Track data.

Arc length (m)	Horizontal curvature (m^{-1})	Super-elevation (m)	Vertical development angle θ (rad)
$s_o = 0.0$	0	0	0
$s_1 = 30.48$	0	0	0
$s_2 = 45.72$	0.00286	0.0381	0.005

using the equation $C_V = \theta'$, which yields $\theta = \theta_o + C_V(s - s_o)$, where θ_o and s_o, are, respectively, the elevation angle and the arc length distance at the first end of the spiral. Knowing the horizontal curvature C_H at the intersection points and assuming linear variation of C_H within the spiral segment, the curvature angle ψ can be determined from the equation $C_H = \psi'/\cos\theta$ as described in the literature (Shabana, Zaazaa and Sugiyama 2008; Shabana 2021).

Recall from Eq. 8 that the position coordinates of the spiral are determined using the integral $\mathbf{r}(s) = \mathbf{r}_o + \int_s \mathbf{r}_s ds = \mathbf{r}_o + \int_s [\cos\psi\cos\theta \quad \sin\psi\cos\theta \quad \sin\theta]^T ds$. Knowing the expressions for the angles ψ and θ, the position coordinates of an arbitrary point on the spiral can be determined without the need for the Frenet bank angle ϕ. This is consistent with the differential-geometry theory that the curve geometry is completely defined by only two geometric invariants; the curvature and twist. Nonetheless, ϕ can be defined in terms of ψ and θ as previously discussed as $\phi = \tan^{-1}(-C_V/C_H\cos^2\theta)$, and consequently, the Frenet bank angle that enters into the definition of the spiral geometry cannot be considered as an independent geometric parameter.

7.2. Spiral-intersection discontinuities

The tangent-spiral-curve track model defined in Table 1 is used as an example to quantify the degree of discontinuity at the tangent/spiral and spiral/curve intersections. Figure 5 shows the curvature, vertical-development (elevation), and Frenet bank angles, ψ, θ, and ϕ, respectively, as functions of the arc length. The results presented in this figure show significant cant discontinuity of the spiral, approximately $\pi/2$, at its intersection with the tangent segment. It is important to point out that the surface of a rail can be further canted to remedy the discontinuity with or without twisting the space curve. In this example, ϕ for the circular curve segment is assumed to be zero (no canting), while ϕ_t is nonzero and has the value that reflects the track super-elevation. The rail surface orientation, which is different from the orientation of the spiral-curve Frenet frame, is used in the definition of the wheel/rail contact forces. Euler angles at the nodal points defined by the track preprocessor using the bank angle ϕ_t and/or the spline data that define the rail profile can be adjusted in order to ensure proper representation of the track geometry. This geometric representation can be conveniently described using the interpolation of the fully-parameterized *absolute nodal coordinate formulation* (ANCF) finite elements which allow for describing the geometry of curves and surfaces (Shabana 2021). Because of the use of more than one position-gradient vector, the ANCF geometric description allows using three independent Euler angles to consistently describe the track geometry and account for the track super-elevation angle based on the linear interpolation of the bank angle. That is, such an ANCF geometric representation, which is based on a surface or volume description, eliminates the inconsistency that results from using three independent angles to describe the curve geometry. Figure 6 shows the horizontal and vertical curvatures C_H and C_V, respectively, as function of the arc length. The results presented in this figure show the discontinuity in the vertical curvature C_V as the result of the spiral twist and vertical elevation. Figure 7 shows the derivative of the track angles with respect to the arc length. For the tangent segment, the derivatives of all angles are zero; and for the curve segments, the derivatives are zero except for the curvature angle ψ, which has constant derivative equal to the horizontal curvature of the curve segment. The results of the torsion along the track, shown in Fig. 8, are consistent with the results of the bank angle previously presented.

The severe discontinuity at the tangent intersection in ϕ shown in Fig. 5 is attributed to the discontinuity of the vertical curvature at this point. A tangent segment has zero vertical curvature, while the spiral has non-zero value. The bank angle algebraic equation $\phi = \tan^{-1}(-C_V/C_H\cos^2\theta)$ explains the source of this discontinuity and the need for developing a better understanding of and a more effective approach for the numerical representation of the track geometry in the computer simulations.
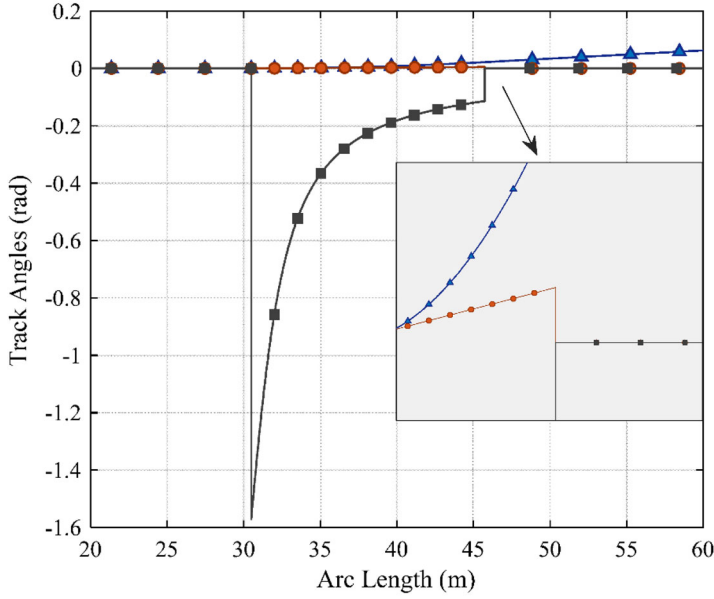
Figure 5. Track angles as functions of the arc length. (—▲— Curvature angle ψ, —●— Vertical-development angle θ, —■— Bank angle ϕ).

As previously mentioned, treating the three Euler angles as independent geometric variables is not consistent with the theory of curves. That is, using an independent linear interpolation of the Frenet bank angle ϕ does not define a space curve; and therefore, it is necessary to distinguish between ϕ and ϕ_t; the latter is used to define the orientation of the nodal track frames to properly account for the track super-elevation, this is with the understanding that ϕ_t is not the Frenet bank angle of the spiral space curve. Figure 8 also shows the torsion τ predicted using a linear interpolation of the bank angle ϕ. This linear interpolation, which is not consistent with the theory of curves and cannot be mathematically justified, is based on using $\phi = 0$ at the tangent/spiral intersection and $\phi = \phi_t$ at the spiral/curve intersection. The limitations of the theory of curves in defining the canting and orientation of the rail surfaces that enter into the wheel/rail contact formulation demonstrate again the need for using ANCF finite elements which allow for changing the orientation of the surfaces without changing the space curve geometric properties (Shabana 2021). Fully-parameterized ANCF finite elements employ three gradient vectors; while a curve has only one gradient vector, making it difficult to have a realistic representation of the track geometry. Furthermore, during the dynamic simulations, the continuity of the ANCF position gradients, including the longitudinal gradient of the space curves, is ensured.

7.3. Normal vector and balance speed

Using the spiral geometric description outlined in this section and using the definition of the curvature vector given by Eq. 5, one can show that the spiral normal vector can be written as

$$\mathbf{n} = \frac{C_H \cos^2\theta}{\kappa} \begin{bmatrix} -\sin\psi \\ \cos\psi \\ 0 \end{bmatrix} + \frac{C_V}{\kappa} \begin{bmatrix} -\cos\psi\sin\theta \\ -\sin\psi\sin\theta \\ \cos\theta \end{bmatrix} \tag{11}$$

This equation shows that the if the vehicle strictly traces the spiral curve, the centrifugal force can be entirely balanced by the component of the gravity force $\mathbf{F}_g^T\mathbf{n} = -(C_V/\kappa)mg\cos\theta$. Using Eq. 3, which shows that $\theta' = C_V = -\kappa\sin\phi$, one has $\mathbf{F}_g^T\mathbf{n} = mg\sin\phi\cos\theta$. Equating this
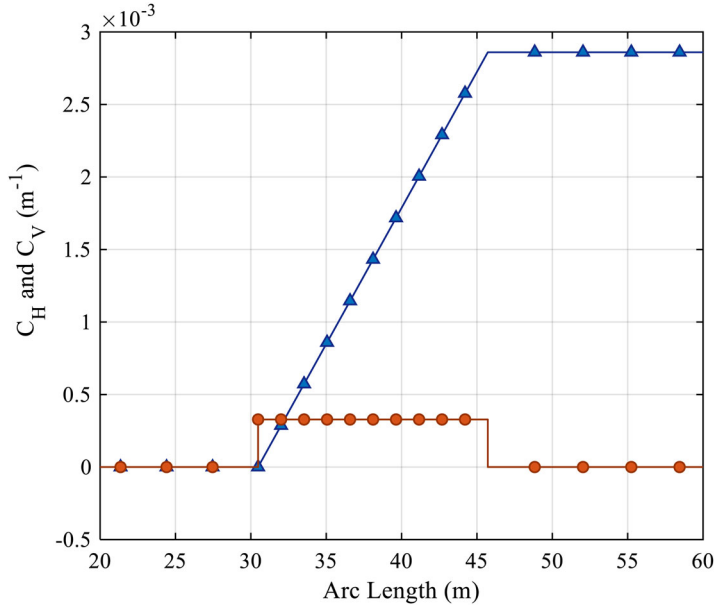
Figure 6. Horizontal and vertical curvatures. (—▲— Horizontal curvature C_H, —●— Vertical curvature C_V).
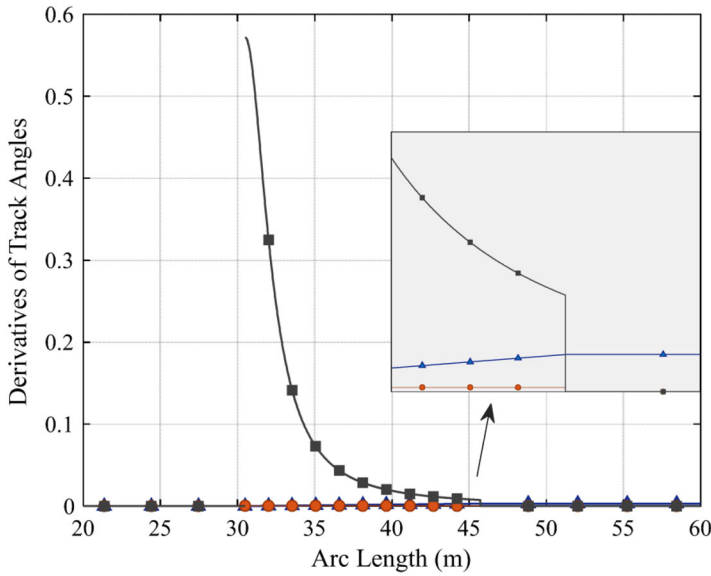

Figure 7. Derivatives of the track angles. (—▲— Curvature angle ψ, —●— Vertical-development angle θ, —■— Bank angle ϕ).

expression with the magnitude of the centrifugal force $m\dot{s}^2/R$, one obtains the balance speed within the spiral as $\dot{s}_b = \sqrt{gR\cos\theta\sin\phi} = \sqrt{(g\cos\theta\sin\phi)/\kappa}$, which is the same as previously presented in this paper. This equation for the balance speed shows dependence on θ and ϕ as well as the curvature κ; all vary within the spiral segment because of the varying curvature and twist, and therefore, the balance speed is not, in general, constant as in the case of the circular curve segment.
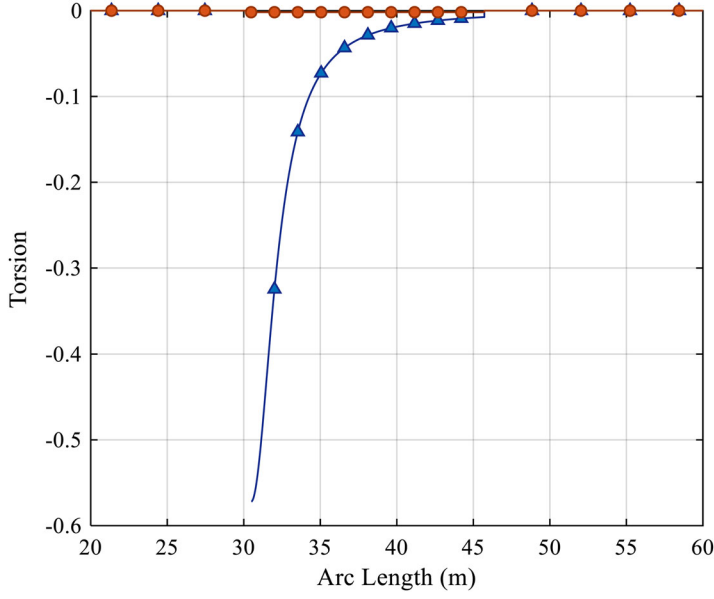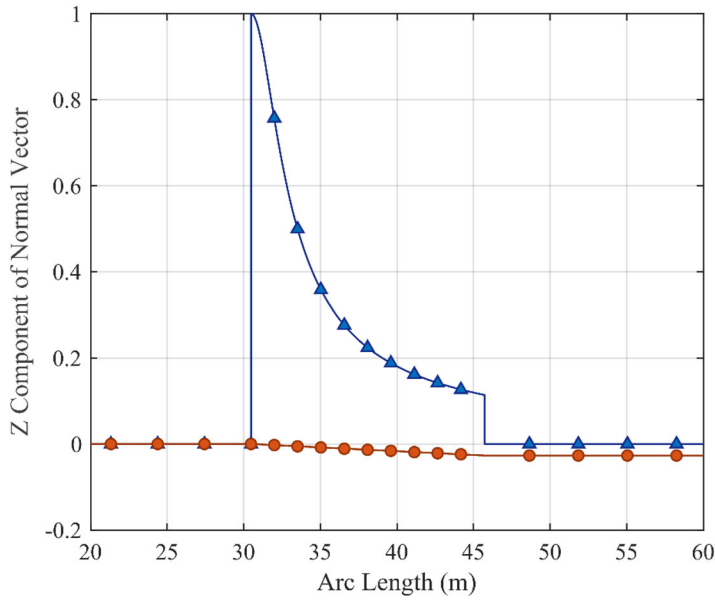
Figure 8. Torsion as function of the arc length. (—▲— algebraically determined bank angle, —●— Linearly interpolated bank angle).
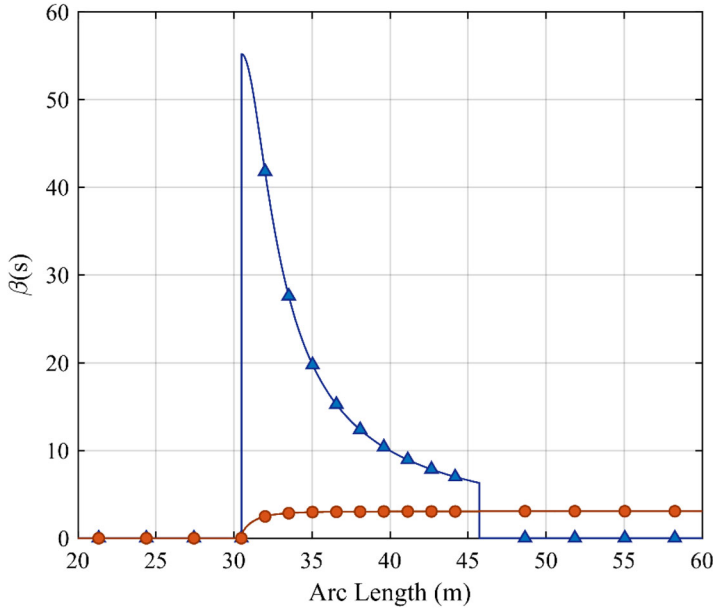
Figure 9. Scaled balance speed $\beta(s)$. (—▲— algebraically determined bank angle, —●— Linearly interpolated bank angle).

In order to quantify the variation of the balance speed within the spiral, the tangent-spiral-curve track example used in a previous study (Ling and Shabana 2020) is considered again. The results of $\beta(s) = \dot{s}_b/\sqrt{g} = \sqrt{(\cos\theta\sin\phi)/\kappa}$, shown in Fig. 9, demonstrate that the balance speed within the spiral does not remain constant. The discontinuities in the balance speed at the spiral intersection with the tangent and curve segments are clear in this figure. However, in Fig. 9, the portion of the linearly-interpolated bank angle that corresponds to the circular curve is taken as

Figure 10. Z component of normal vector as function of arc length. (—▲— algebraically determined bank angle, —●— Linearly interpolated bank angle).

ϕ_t to show the continuity if this angle is used. Figure 9 also shows the scaled balance speed β when ϕ is linearly interpolated and treated as an independent variable. Figure 10 shows the vertical component of the normal vector when ϕ is treated as dependent and independent parameters. This vertical component shows the deviation from a completely horizontal centrifugal force.

8. Summary and conclusions

The pre-defined track geometry is used to define the balance speed because the actual motion-trajectory curves are not a priori known. Because of the small value of the super-elevation angle, the analysis presented in this paper can be used to demonstrate that such an approximation of the balance speed is acceptable in most practical railroad vehicle system applications (Schupp 2003). However, because of the lack of a geometric approach that can be used to characterize and quantify the railroad track-transition discontinuities and lack of understanding of the variation of the bank angle and vertical-elevation within the spiral segments, it is not possible to develop a science-based technique for determining the balance speed, smoothing the transition discontinuities, and/or developing credible operation and safety guidelines for avoiding serious accidents and derailments. For this reason, this study builds on a previous investigation by the authors (Ling and Shabana 2020) by developing a new approach for the characterization and quantification of the spiral-intersection discontinuities as well as developing a more accurate definition of the balance speed. In order to develop understanding of the geometry, three different curves which have fundamentally different geometries are considered; a super-elevated *constant-curvature curve* with zero twist and zero vertical elevation, a vertically-elevated *helix curve* with a constant curvature and twist and zero bank angle, and a *spiral curve* with non-zero varying-curvature, twist, bank angle, and vertical elevation. The curve equations are developed in terms of Euler angles used by the rail industry to describe the track geometry in the computer simulations. As discussed in this paper, the spiral geometry can be completely defined in terms of the *horizontal-curvature* and the *vertical-development* angles only. Therefore, the Frenet bank angle, which is written in terms of these two angles, cannot be treated as an independent variable. The results obtained in this investigation demonstrate that, when the spiral is twisted and elevated, the

super-elevation discontinuities can be large at the intersections if no smoothing measures are taken. The numerical results obtained demonstrate the problem of interpreting independent linear interpolation of the bank angle used in the railroad computer algorithms as the Frenet bank angle that enters into the definition of the geometry of the spiral space curve. These results, which show high degree of transition discontinuities, should be used in a qualitative assessment because a purely geometric analysis does not take into account practical considerations used in the actual layout of the track and because the discontinuities of the space curves can be different from discontinuities at the rail surfaces whose geometries enter into the definitions of the wheel/rail contact forces. Future investigations will be focused on demonstrating the significance of the concepts discussed in this paper using multibody system (MBS) simulation techniques (Fisette et al. 2002; Shabana 2021).

Acknowledgements

Funding

References

Andersson, C., and T. Abrahamsson. 2002. Simulation of interaction between a train in general motion and a track. *Vehicle System Dynamics* 38 (6):433–55. doi:10.1076/vesd.38.6.433.8345.

Berghuvud, A. 2002. Freight car curving performance in braked conditions. Proceedings of the Institution of Mechanical Engineers, Part F: Journal of Rail and Rapid Transit 216 (1):23–9. doi:10.1243/0954409021531656.

Blue, D. W., and B. T. Kulakowski. 1991. Effects of horizontal-curve transition design on truck roll stability. *Journal of Transportation Engineering* 117 (1):91–102. doi:10.1061/(ASCE)0733-947X(1991)117:1(91).

De Pater, A. D. 1988. The geometrical contact between track and wheelset. *Vehicle System Dynamics* 17 (3):127–40. doi:10.1080/00423118808968898.

Do Carmo, M. P. 1976. *Differential geometry of curves and surfaces*. Englewood Cliffs, NJ: Prentice Hall.

Elkins, J. A., and R. J. Gostling. 1977. A general quasi-static curving theory for railway vehicles. *Vehicle System Dynamics* 6 (2–3):100–6. doi:10.1080/00423117708968515.

Endlicher, K. O., and P. Lugner. 1990. Computer simulation of the dynamical curving behavior of a railway bogie. *Vehicle System Dynamics* 19 (2):71–95. doi:10.1080/00423119008968934.

Fisette, P., T. Postiau, L. Sass, and J. C. Samin. 2002. Fully symbolic generation of complex multibody models. *Mechanics of Structures and Machines* 30 (1):31–82. doi:10.1081/SME-120001477.

Gailienė, I. 2012. Investigation into the calculation of superelevation defects on conventional rail lines. *TRANSPORT* 27 (3):229–36. doi:10.3846/16484142.2012.719198.

Gilchrist, A. O. 1998. The long road to solution of the railway hunting and curving problems. Proceedings of the Institution of Mechanical Engineers, Part F: Journal of Rail and Rapid Transit 212 (3):219–26. doi:10.1243/0954409981530814.

Goetz, A. 1970. *Introduction to differential geometry*. Boston, MA: Addison Wesley.

Grassie, S. L. 1993. Dynamic modeling of the track and their uses. In *Rail quality and maintenance for modern railway operation*, ed. J. J. Kalker, D. F. Cannon, and O. Orringer, 165–84. Dordrecht: Kluwer.

Hamid, A., K. Rasmussen, M. Baluja, and T.-L. Yang. 1983. Analytical description of track geometry variations. DOT/FRA/ORD-83/03.1, Federal Railroad Administration, Springfield, VA.

Handoko, Y., F. Xia, and M. Dhanasekar. 2004. Effect of asymmetric brake shoe force application on wagon curving performance. *Vehicle System Dynamic Dynamics* 41:113–22.

Jalili, M. M., M. Motavasselolhagh, R. Fatehi, and M. Sefid. 2020. Investigation of sloshing effects on lateral stability of tank vehicles during turning maneuver. *Mechanics Based Design of Structures and Machines*. doi:10.1080/15397734.2020.1800490.

Kerr, A. D., and M. A. El-Sibaie. 1987. On the new equations for the lateral dynamics of rail-tie structure. *ASME Journal of Dynamic Systems, Measurement, and Control* 107:180–5.

Kik, W. 1992. Comparison of the behavior of different wheelset-track models. *Vehicle System Dynamics* 20 (sup1):325–39. doi:10.1080/00423119208969407.

Klauder Jr, L. T. 2012. Railroad spiral design and performance. ASME/IEEE Joint Rail Conference 44656, 9–21. New York: American Society of Mechanical Engineers.

Klauder Jr, L. T., S. M. Chrismer, and J. Elkins. 2002. Improved spiral geometry for high-speed rail and predicted vehicle response. *Transportation Research Record: Journal of the Transportation Research Board* 1785 (1):41–9. doi:10.3141/1785-06.

Knothe, K. L., and S. L. Grassie. 1993. Modeling of railway track and vehicle/track interaction at high frequencies. *Vehicle System Dynamics* 22 (3–4):209–62. doi:10.1080/00423119308969027.

Knothe, K. L., and S. Stichel. 1994. Direct covariance analysis for the calculation of creepages and creep-forces for various bogie on straight track with random irregularities. *Vehicle System Dynamics* 23 (1):237–51. doi:10.1080/00423119408969058.

Kreyszig, E. 1991. *Differential geometry.* New York: Dover Publications.

Ling, H., and A. A. Shabana. 2020. *Numerical representation of railroad track geometry using Euler angles. Acta Mechanica* (in press).

Liu, Y., and E. Magel. 2009. Performance-based track geometry and the track geometry interaction map. *Proceedings of the Institution of Mechanical Engineers, Part F: Journal of Rail and Rapid Transit* 223 (2):111–9. doi:10.1243/09544097JRRT225.

Magel, E., P. Sroba, K. Sawley, and J. Kalousek. 2005. Control of rolling contact fatigue of rails. Center for Surface Transportation Technology, National Research Council Canada.

Pascal, J. P., and J. R. Sany. 2019. Dynamics of an isolated railway wheelset with conformal wheel–rail interactions. *Vehicle System Dynamics* 57 (12):1947–69. doi:10.1080/00423114.2018.1557704.

Prud'home, A. 1978. Forces and behavior of railroad tracks at very high train speeds; standards adopted by SNCF for its future high speed lines (250 to 300 km/h). In *Railroad Track Mechanics and Technology*, ed. A. D. Kerr, 79–108. Oxford, UK: Pergamon Press.

Schupp, G. 2003. Simulation of railway vehicles: Necessities and applications. *Mechanics Based Design of Structures and Machines* 31 (3):297–314. doi:10.1081/SME-120022852.

Shabana, A. A. 2021. *Mathematical foundation of railroad vehicle systems: Geometry and mechanics.* Hoboken, NJ: Wiley & Sons.

Shabana, A. A., and H. Ling. 2019. Noncommutativity of finite rotations and definitions of curvature and torsion. *Journal of Computational and Nonlinear Dynamics* 14 (9):091005. doi:10.1115/1.4043726.

Shabana, A. A., K. E. Zaazaa, and H. Sugiyama. 2008. *Railroad Vehicle Dynamics: A Computational Approach.* Boca Raton, FL: CRC Press.

True, H. 1994. Does a critical speed for railroad vehicles exist? In *Proceedings of IEEE/ASME Joint Railroad Conference*, 125–31.

Wickens, A. 2005. *Fundamentals of rail vehicle dynamics.* Boca Raton, FL: CRC Press.

Zhang, Y., M. A. El-Sibaie, and S. Lee. 2004. FRA track quality indices and distribution characteristics. AREMA 2004 Annual Conference, Nashville, TN, September 19.

Appendix A

Super-elevation and centrifugal forces

A surface, including the rail track plane, is parametrized using two coordinates. As shown in this paper, the absolute acceleration vector of a mass that traces a curve has two components, one along the tangent vector and the other along the vector normal to the curve; that is, the absolute acceleration vector always lies in the *osculating plane*. In general, the orientation of the osculating plane changes during the course of motion. In this appendix, two cases are considered in order to demonstrate the procedure for determining the centrifugal forces.

A.1.   Super-elevation

In this section, a simple example is used to explain the difference between the super-elevation of a surface and the direction of the centrifugal force which is along the normal to the motion-trajectory curve on the surface. Figure 11 shows a surface which makes an angle ϕ_t with the horizontal plane. The figure shows a circular curve C that lies on a plane parallel to the horizontal plane; that is, this circular curve is the intersection of the surface and a horizontal planar surface. As previously mentioned, if a mass strictly follows this horizontal circular curve, the centrifugal force remains in the horizontal plane along the vector $\mathbf{n}_C$ normal to curve. If the mass, on the other hand, moves laterally with a displacement y along the axis Y_t in addition to the forward motion on the surface, the mass traces another curve D, shown in the figure. This lateral displacement y, which can represent hunting oscillations, sliding toward the low rail, and/or lateral wheel climb displacements in railroad vehicle systems; is measured with respect to the circle C. The actual *motion plane* at an arbitrary point on curve D, which is the *osculating plane*

formed by the tangent vector $\mathbf{t}_D$ and the normal vector $\mathbf{n}_D$, is shown in the figure. The analysis presented in this section shows that this motion plane is, in general, different from the plane tangent to the surface, that is the normal vector $\mathbf{n}_D$ does not in general lie on the tangent plane of the surface which has the curve D. Using Fig. 11, one can show that the global position vector of a point that traces the curve D can be written as

$$\mathbf{r} = \begin{bmatrix} R \sin \psi \\ -R \cos \psi \\ Z_C \end{bmatrix} + y \begin{bmatrix} \cos \phi_t \sin \psi \\ \cos \phi_t \cos \psi \\ -\cos \phi_t \end{bmatrix} = \begin{bmatrix} (R - y \cos \phi_t) \sin \psi \\ -(R - y \cos \phi_t) \cos \psi \\ Z_C - y \sin \phi_t \end{bmatrix} \tag{A.1}$$

where Z_C is a constant that defines the elevation of the horizontal circle C, R is the radius of the curve, $\psi = S/R$ is the curvature angle of the circle C, and S is the arc length of the circle. If s is the arc length of the motion-trajectory curve D, one can define the unit tangent vector to this curve as

$$\mathbf{r}_s = \frac{\partial \mathbf{r}}{\partial s} = \begin{bmatrix} \psi_s(R - y \cos \phi_t) \cos \psi - y_s \cos \phi_t \sin \psi \\ \psi_s(R - y \cos \phi_t) \sin \psi + y_s \cos \phi_t \cos \psi \\ -y_s \sin \phi_t \end{bmatrix} \tag{A.2}$$

where $a_s = \partial a / \partial s$. The fact that the tangent vector $\mathbf{r}_s$ in the preceding equation is a unit vector can be used to define the following relationship between ψ_s and y_s:

$$(\psi_s)^2(R - y \cos \phi_t)^2 + (y_s)^2 = 1 \tag{A.3}$$

This equation shows that

$$\psi_{ss}\psi_s(R - y \cos \phi_t)^2 + y_{ss}y_s = (\psi_s)^2 y_s \cos \phi_t (R - y \cos \phi_t) \tag{A.4}$$

The curvature vector which defines the direction of the centrifugal force is defined as

$$\mathbf{r}_{ss} = \frac{\partial^2 \mathbf{r}}{\partial s^2} = \begin{bmatrix} (\psi_{ss} \cos \psi - (\psi_s)^2 \sin \psi)(R - y \cos \phi_t) - 2\psi_s y_s \cos \phi_t \cos \psi - y_{ss} \cos \phi_t \sin \psi \\ (\psi_{ss} \sin \psi + (\psi_s)^2 \cos \psi)(R - y \cos \phi_t) - 2\psi_s y_s \cos \phi_t \sin \psi + y_{ss} \cos \phi_t \cos \psi \\ -y_{ss} \sin \phi_t \end{bmatrix} \tag{A.5}$$

The norm of this curvature vector defines the curvature $\kappa = 1/R_D$ of the motion trajectory curve, where $R_D = R_D(s)$ is the radius of curvature of the curve D. The unit normal to the curve D is defined as $\mathbf{n} = (1/\kappa)\mathbf{r}_{ss}$, and the magnitude of the centrifugal force along this normal is $\dot{s}^2/R_D$. It is clear from this equation and the preceding equation that the curvature vector has non-zero vertical component $-y_{ss} \sin \phi_t / \kappa$, which depends on the geometric properties of the curve D as well as the super-elevation of the surface. Increasing the surface super-elevation and y_{ss} makes the direction of the centrifugal force further deviates from the horizontal plane.

On the other hand, if the arc length S of the horizontal circle is considered as the curve parameter, one has

$$\dot{\mathbf{r}} = \mathbf{r}_S\dot{S} = \begin{bmatrix} \psi_S(R - y \cos \phi_t) \cos \psi - y_S \cos \phi_t \sin \psi \\ \psi_S(R - y \cos \phi_t) \sin \psi + y_S \cos \phi_t \cos \psi \\ -y_S \sin \phi_t \end{bmatrix} \dot{S} \tag{A.6}$$

where in this equation $a_S = \partial a / \partial S$. The norm of the vector $\mathbf{r}_S$ is

$$\beta = |\mathbf{r}_S| = \sqrt{(\psi_S)^2(R - y \cos \phi_t)^2 + (y_S)^2} \tag{A.8}$$

It is clear from this equation that if $y = 0$, $\beta = 1$. The relationship between the actual arc length of the motion trajectory curve s and the arc length of the horizontal circle S is $ds = \beta dS$, that is, $ds/dS = \beta$ and $\dot{s} = \beta\dot{S}$. It follows that $\ddot{s} = \beta\ddot{S} + \dot{\beta}\dot{S}$. One can also write

$$\ddot{S} = (\ddot{s}\beta - \dot{s}\dot{\beta})/\beta^2 \tag{A.9}$$

Using these definitions, it is clear that $y_s = (\partial y / \partial S)/\beta$ and

$$y_{ss} = \left(\frac{1}{\beta}\right) \frac{\partial[(\partial y / \partial S)/\beta]}{\partial S} = \left(\frac{1}{\beta^3}\right)(y_{SS}\beta - y_S\beta_S) \tag{A.10}$$

As an example, consider the case in which $y = Y_o \sin \alpha S$, where Y_o and α are constants. It follows that

$$\left. \begin{array}{ll} \psi_S = 1/R, & \psi_{SS} = 0, \\ y_S = \alpha Y_o \cos \alpha S, & y_{SS} = -\alpha^2 Y_o \sin \alpha S \end{array} \right\} \tag{A.11}$$

In this case, one has

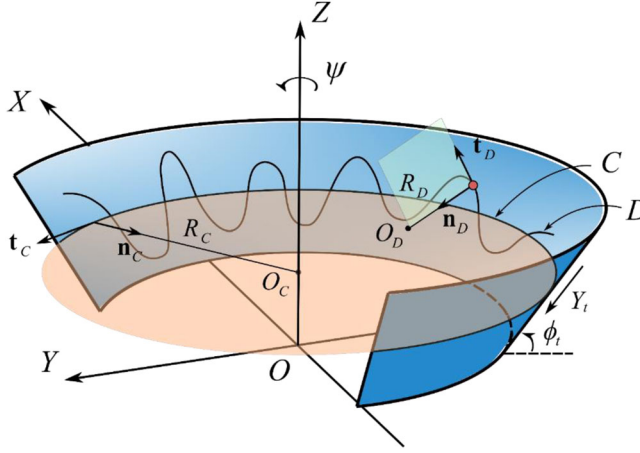**Figure 11.** Motion trajectories.

$$\beta = |\mathbf{r_S}| = \sqrt{\left((R - Y_o \sin \alpha S \cos \phi_t)/R\right)^2 + (\alpha Y_o \cos \alpha S)^2} \tag{A.12}$$

Using this definition, one can write

$$\dot{s} = \beta \dot{S} = \left(\sqrt{\left((R - Y_o \sin \alpha S \cos \phi_t)/R\right)^2 + (\alpha Y_o \cos \alpha S)^2}\right) \dot{S} \tag{A.13}$$

It is clear from the preceding equations that if the frequency α is large, $\dot{s}$ can vary significantly from $\dot{S}$ and the direction of the centrifugal force deviates from the horizontal plane. Furthermore, using the analysis presented in this paper, the Frenet bank angle ϕ of the curve can be determined by equating the expression of the normal vector obtained in this section to the general expression previously presented in this paper as $\mathbf{n} = \left[(-\sin \psi \cos \phi + \cos \psi \sin \theta \sin \phi) \quad \cos \psi \cos \phi + \sin \psi \sin \theta \sin \phi \quad -\cos \theta \sin \phi\right]^T$. Assuming that ψ is the same for both descriptions; one, by equating the expressions of the normal vectors, can define the vertical-elevation and Frenet bank angles θ and ϕ, respectively. For example, one has the following relationship by equating the vertical components of the two normal vectors: $y_{ss} \sin \phi_t = \cos \theta \sin \phi$.

A.2. Conical surface

The cone example used to draw a similarity with the super-elevated curved track is used in this section to shed light on some fundamental geometric issues in the definition of the inertia forces. The cone surface is defined as a surface of revolution generated by rotating an inclined line in the vertical plane about the vertical axis. The angles used to generate the cone geometry do not follow the same sequence of rotations as the sequence used to define the super-elevated track geometry, and therefore, the inclination of the cone surface needs to be properly interpreted. Figure 12 shows a vector that makes an angle ϕ_c with the vertical axis Z. This angle ϕ_c, which is assumed constant, is half the cone angle and is equal to $\phi_c = (\pi/2) - \phi$, where ϕ is the angle of rotation about the $-X$ axis as shown in the figure. If y is defined to be the coordinate of a point along the vector shown in the figure, one can define the Cartesian coordinates of this point as $\mathbf{v}_c = y\begin{bmatrix}0 & -\sin \phi_c & \cos \phi_c\end{bmatrix}^T$. To generate the cone surface, the vector $\mathbf{v}_c$ is rotated by angle ψ about the Z axis. This rotation defines the cone surface in terms of the two parameters y and ψ. The position and velocity vectors of an arbitrary point on the cone surface are defined as

$$\mathbf{r} = y\begin{bmatrix} \sin \psi \sin \phi_c \\ -\cos \psi \sin \phi_c \\ \cos \phi_c \end{bmatrix}, \quad \dot{\mathbf{r}} = \dot{y}\begin{bmatrix} \sin \psi \sin \phi_c \\ -\cos \psi \sin \phi_c \\ \cos \phi_c \end{bmatrix} + y\dot{\psi}\begin{bmatrix} \cos \psi \sin \phi_c \\ \sin \psi \sin \phi_c \\ 0 \end{bmatrix} \tag{A.14}$$

These vectors can be written as

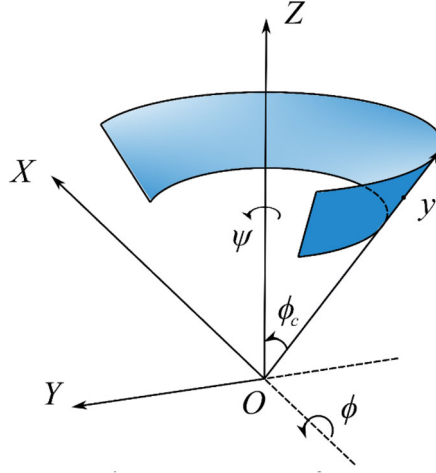**Figure 12.** Cone surface.

$$\mathbf{r} = R_c \begin{bmatrix} \sin\psi \\ -\cos\psi \\ 1/\tan\phi_c \end{bmatrix},$$

$$\dot{\mathbf{r}} = \dot{R}_c \begin{bmatrix} \sin\psi \\ -\cos\psi \\ 1/\tan\phi_c \end{bmatrix} + R_c\dot\psi \begin{bmatrix} \cos\psi \\ \sin\psi \\ 0 \end{bmatrix} = \begin{bmatrix} R_c\cos\psi & \sin\psi \\ R_c\sin\psi & -\cos\psi \\ 0 & 1/\tan\phi_c \end{bmatrix} \begin{bmatrix} \dot\psi \\ \dot{R}_c \end{bmatrix} \tag{A.15}$$

where $R_c = y\sin\phi_c$. The unit normal to the cone surface is

$$\mathbf{n} = \begin{bmatrix} \sin\psi\cos\phi_c & -\cos\psi\cos\phi_c & -\sin\phi_c \end{bmatrix}^T \tag{A.16}$$

For a given circle on the cone surface, one has $s_c = \psi y\sin\phi_c$, which leads to $\dot{s}_c = (\dot\psi y + \psi\dot{y})\sin\phi_c = R_c\dot\psi + \dot{R}_c\psi$. One can then write

$$\begin{bmatrix} \dot\psi \\ \dot{R}_c \end{bmatrix} = \begin{bmatrix} 1 & 0 \\ 0 & \sin\phi_c \end{bmatrix} \begin{bmatrix} \dot\psi \\ \dot{y} \end{bmatrix}, \quad \dot{\mathbf{r}} = \begin{bmatrix} R_c\cos\psi & \sin\psi\sin\phi_c \\ R_c\sin\psi & -\cos\psi\sin\phi_c \\ 0 & \cos\phi_c \end{bmatrix} \begin{bmatrix} \dot\psi \\ \dot{y} \end{bmatrix} \tag{A.17}$$

The acceleration vector is defined as

$$\ddot{\mathbf{r}} = \ddot{y} \begin{bmatrix} \sin\psi\sin\phi_c \\ -\cos\psi\sin\phi_c \\ \cos\phi_c \end{bmatrix} + \left(2\dot{y}\dot\psi + y\ddot\psi\right) \begin{bmatrix} \cos\psi\sin\phi_c \\ \sin\psi\sin\phi_c \\ 0 \end{bmatrix} + y\dot\psi^2 \begin{bmatrix} -\sin\psi\sin\phi_c \\ \cos\psi\sin\phi_c \\ 0 \end{bmatrix} \tag{A.18}$$

Or alternatively,

$$\ddot{\mathbf{r}} = \ddot{R}_c \begin{bmatrix} \sin\psi \\ -\cos\psi \\ 1/\tan\phi_c \end{bmatrix} + \left(2\dot{R}_c\dot\psi + R_c\ddot\psi\right) \begin{bmatrix} \cos\psi \\ \sin\psi \\ 0 \end{bmatrix} + R_c\dot\psi^2 \begin{bmatrix} -\sin\psi \\ \cos\psi \\ 0 \end{bmatrix} \tag{A.19}$$

Balancing the inertia force in the lateral direction requires accurate interpretation of the inertia forces that appear in the preceding equation. For this reason, the correct definition of the centrifugal force based on the motion-trajectory curve is developed in the following section.

A.3. *Motion-trajectory curves*

The centrifugal force is defined along the unit vector normal to a motion-trajectory curve. In order to properly define such a curve on a surface, the two surface parameters need to be written in terms of one parameter. In this section, the cone surface is used as an example to demonstrate how the direction of the centrifugal force is defined.

To this end, the surface parameters ψ and y are written, respectively, in terms of the arc length s of the motion-trajectory curve as $\psi = \psi(s)$ and $y = y(s)$. In this case, one has

$$\begin{bmatrix} \dot{\psi} & \dot{y} \end{bmatrix}^T = \begin{bmatrix} \partial\psi/\partial s & \partial y/\partial s \end{bmatrix}^T \dot{s} = \begin{bmatrix} \psi_s & y_s \end{bmatrix}^T \dot{s} \tag{A.20}$$

Using this equation, the equation of the curve on the cone surface and the velocity vector can be written, respectively, as

$$\mathbf{r} = y \begin{bmatrix} \sin\psi \sin\phi_c \\ -\cos\psi \sin\phi_c \\ \cos\phi_c \end{bmatrix}, \quad \dot{\mathbf{r}} = \begin{bmatrix} y_s \sin\psi \sin\phi_c + y\psi_s \cos\psi \sin\phi_c \\ -y_s \cos\psi \sin\phi_c + y\psi_s \sin\psi \sin\phi_c \\ y_s \cos\phi_c \end{bmatrix} \dot{s} = \mathbf{r}_s \dot{s} \tag{A.21}$$

where the vector $\mathbf{r}_s$ is the unit tangent to the curve defined as

$$\mathbf{r}_s = \frac{\partial\mathbf{r}}{\partial s} = \begin{bmatrix} y_s \sin\psi \sin\phi_c + y\psi_s \cos\psi \sin\phi_c \\ -y_s \cos\psi \sin\phi_c + y\psi_s \sin\psi \sin\phi_c \\ y_s \cos\phi_c \end{bmatrix} \tag{A.22}$$

This vector, which defines in the case of railroad vehicle systems the direction of motion and traction forces, always lies on tangent plane to the surface. One can show that this vector is a linear combination of the two vectors tangent to the surface. The fact that the vector $\mathbf{r}_s$ is a unit vector shows that a curve on the cone surface must satisfy the equation

$$y_s^2 + y^2\psi_s^2 \sin^2\phi_c = 1 \tag{A.23}$$

The curvature vector can be obtained by differentiating the unit tangent vector with respect to the arc length. This leads to

$$\mathbf{r}_{ss} = \frac{\partial\mathbf{r}_s}{\partial s} = \begin{bmatrix} (y_{ss} - y\psi_s^2) \sin\psi \sin\phi_c + (2y_s\psi_s + y\psi_{ss}) \cos\psi \sin\phi_c \\ -(y_{ss} - y\psi_s^2) \cos\psi \sin\phi_c + (2y_s\psi_s + y\psi_{ss}) \sin\psi \sin\phi_c \\ y_{ss} \cos\phi_c \end{bmatrix}$$

$$= y_{ss} \begin{bmatrix} \sin\psi \sin\phi_c \\ -\cos\psi \sin\phi_c \\ \cos\phi_c \end{bmatrix} - R_c\psi_s^2 \begin{bmatrix} \sin\psi \\ -\cos\psi \\ 0 \end{bmatrix} + (2y_s\psi_s + y\psi_{ss}) \sin\phi_c \begin{bmatrix} \cos\psi \\ \sin\psi \\ 0 \end{bmatrix} \tag{A.24}$$

The norm of this vector defines the curve curvature κ as

$$\kappa = 1/R = \sqrt{(\kappa_h \sin\phi_c)^2 + (\kappa_v \cos\phi_c)^2} \tag{A.25}$$

where R is the radius of curvature of the curve, $\kappa_h = \sqrt{(y_{ss} - y\psi_s^2)^2 + (2y_s\psi_s + y\psi_{ss})^2}$, and $\kappa_v = y_{ss}$. The unit normal vector is then defined as $\mathbf{n} = (1/\kappa)\mathbf{r}_{ss}$, or more explicitly as

$$\mathbf{n} = \frac{1}{\kappa} \begin{bmatrix} (y_{ss} - y\psi_s^2) \sin\psi \sin\phi_c + (2y_s\psi_s + y\psi_{ss}) \cos\psi \sin\phi_c \\ -(y_{ss} - y\psi_s^2) \cos\psi \sin\phi_c + (2y_s\psi_s + y\psi_{ss}) \sin\psi \sin\phi_c \\ y_{ss} \cos\phi_c \end{bmatrix} \tag{A.26}$$

Unlike the tangent vector, it is clear that this normal vector does not always lie on the tangent plane of the cone surface. From the definition of the inertia force vector $\mathbf{F}_i = \ddot{s}\mathbf{r}_s + (\dot{s}^2/R)\mathbf{n}$, it is clear that the centrifugal force is not in the horizontal plane, unless $y_{ss} = 0$. In railroad system applications, there is no guarantee that y_{ss} is small in the case of hunting oscillations which can happen at high frequencies, particularly in the case of wheel flange impacts with the rail. As previously mentioned with reference to Fig. 2, the variation of the curvature angle ψ of a circular curve on the cone surface with respect to the arc length s of the motion-trajectory curve will always be smaller than the variation of the same angle with respect to the arc length of the circle. That is, if s_c is the arc length of a horizontal circle on the cone surface, one always has $\psi_s = \partial\psi/\partial s < \psi_{s_c} = \partial\psi/\partial s_c$. Furthermore, in most railroad system applications, the radius of curvature of the curve segment is assumed large, and therefore, ψ_{s_c} is small. As ψ_{s_c} decreases by using a larger radius of curvature and as the hunting frequency increases, the dominant component of the normal vector and the centrifugal force vector will lie in a plane closer to the tangent plane of the surface and will shift away from the horizontal plane.